Direct Visualization of Valence Electron Motion Using Strong-Field Photoelectron Holography

Mingrui He,[1] Yang Li,[1] Yueming Zhou,[1,*] Min Li,[1] Wei Cao,[1] and Peixiang Lu[1,2,†]
[1]School of Physics and Wuhan National Laboratory for Optoelectronics, Huazhong University of Science and Technology, Wuhan 430074, China
[2]Laboratory of Optical Information Technology, Wuhan Institute of Technology, Wuhan 430205, China

(Received 13 October 2017; published 28 March 2018)

Watching the valence electron move in molecules on its intrinsic timescale has been one of the central goals of attosecond science and it requires measurements with subatomic spatial and attosecond temporal resolutions. The time-resolved photoelectron holography in strong-field tunneling ionization holds the promise to access this realm. However, it remains to be a challenging task hitherto. Here we reveal how the information of valence electron motion is encoded in the hologram of the photoelectron momentum distribution (PEMD) and develop a novel approach of retrieval. As a demonstration, applying it to the PEMDs obtained by solving the time-dependent Schrödinger equation for the prototypical molecule H_2^+, the attosecond charge migration is directly visualized with picometer spatial and attosecond temporal resolutions. Our method represents a general approach for monitoring attosecond charge migration in more complex polyatomic and biological molecules, which is one of the central tasks in the newly emerging attosecond chemistry.

DOI: 10.1103/PhysRevLett.120.133204

Monitoring electron motion in atoms and molecules on its natural attosecond (1 as $= 10^{-18}$ s) timescale with sub-Ångström spatial resolution is essential for understanding and steering chemical reactions and biological processes. While the methods of x-ray and electron diffraction are routinely employed to achieve sub-Ångström spatial resolution, their current temporal resolution is not applicable of monitoring attosecond dynamics. Recent progress in attosecond technology has allowed the measurement with attosecond temporal resolution, as illustrated by the experiments of attosecond transient absorption [1,2], attosecond streaking [3,4], and attosecond electron wave packet interferometry [5–8]. Alternatively, the measurements based on laser-induced recollision in strong-field ionization also access attosecond resolution and have been widely explored to trace the ultrafast dynamics in atoms and molecules [9–15]. In particular, the so-called laser-induced electron diffraction possesses the combined subatomic and (sub-)femtosecond resolutions and has been used to probe the ultrafast nuclear dynamics in molecules [16,17]. However, the attosecond electronic dynamics has so far escaped observation with this laser-induced electron diffraction, due to its insensitivity on the structure of the valence electrons [18,19]. Here, we demonstrate that another type of recollision-based measurement, time-resolved strong-field photoelectron holography (SFPH), possesses the combined subatomic spatial and attosecond temporal resolutions and can be used to monitor ultrafast valance-shell electronic dynamics in real time.

The interference pattern of SFPH in photoelectron momentum distributions (PEMDs) has been experimentally observed for different targets [20–23]. Theoretical analysis has recognized this interference results from electrons flying directly to the detector after tunneling ionization and those undergoing near-forward rescattering by the parent ion [20]. It was suggested that these holograms encode structural as well as dynamic information of the targets. Previously, we have elucidated the extraction of the structural information [24]. The imprint of molecular attosecond electronic dynamics on the holograms has been experimentally reported very recently [19,25]. However, the retrieval of the dynamic information remains unsolved. Here, we show how the dynamic information of the valence electron is encoded in the holographic pattern and demonstrate a scheme of retrieval. We illustrate that with this scheme the attosecond migration of the valence electron wave packet is directly visualized with spatial resolution of 10^{-12} m and temporal resolution of 10^{-18} s in a single-shot measurement. This work represents a general approach for real-time and *in situ* monitoring of the ultrafast electron dynamics in atoms and molecules with unprecedented spatio-temporal resolution.

We illustrate our scheme by considering the simplest system of H_2^+. The electronic dynamics is induced by the coherent superposition of two electronic states $\psi(\mathbf{r},t) = c_1\psi_1(\mathbf{r})e^{-iE_1t/\hbar} + c_2\psi_2(\mathbf{r})e^{-i(E_2t/\hbar+\theta_0)}$, where $\psi_1(\mathbf{r})$ and $\psi_2(\mathbf{r})$ are the ground ($1s\sigma_g$) and first excited ($2p\sigma_u$) electronic states of H_2^+. c_1, c_2 are the corresponding

expansion coefficients and θ_0 is the initial relative phase of the two states. We start our calculations from this superposition state. Experimentally, the superposition state could be prepared by a pump pulse with the resonant frequency, and the initial phase θ_0 is adjustable by changing pump-probe delay. In our calculations, we solve the two-dimensional time-dependent Schrödinger equation for a two-center soft-core potential modeling H_2^+ [26], where the fixed internuclear distance of $R_0 = 4$ a.u. is adopted because the electronic dynamics we focused on here is within a time interval of several hundreds attoseconds during which the nuclear motion can be neglected. The soft-core parameter is adjusted to give ionization energies of $E_1 = 21.7$ eV for the ground and $E_2 = 17.8$ eV for the first excited state, which leads to a period of $\tau = 2\pi/\Delta E = 1.056$ fs for the oscillation of the superposition-state electron wave packet. A linearly polarized single-cycle model pulse with the intensity of 3.0×10^{14} W/cm^2 is adopted to ionize H_2^+. The wavelength of laser pulse is chosen to be 2000 nm instead of the usual 800 nm to minimize the nonadiabatic effect associated with ionization or excitation and also to ensure a wider time window for tunneling ionization. In the single-cycle model pulse, the recollision process is especially simple, which is benefit for illustrating the essence of our scheme. The result for the realistic few-cycle laser pulse is shown in Ref. [26].

Figure 1 shows the PEMDs for strong-field ionization of H_2^+ by the single-cycle model pulse where the molecule is aligned perpendicular to the laser polarization direction ($\hat{z}$ axis). Figures 1(a) and 1(b) present the results for ionization from the ground state and the nonstationary superposition state with $c_2/c_1 = 0.5$ and $\theta_0 = 0$, respectively. Two types of interference fringes can be observed. The nearly vertical ones are the interference of the direct electrons tunneling ionized during two adjacent half cycles [36]. The other nearly horizontal fringes are the holographic structure that we will focus on. For the stationary $1s\sigma_g$ state, the holographic fringes are exactly symmetric about $k_\perp = 0$. While for the nonstationary superposition state, the positions of the interference minima and maxima in the hologram are obviously asymmetric with respect to $k_\perp = 0$. Moreover, this asymmetry changes with k_z. As we will show, this asymmetry and its k_z dependence record the coherent electronic dynamics of the superposition state on attosecond timescale.

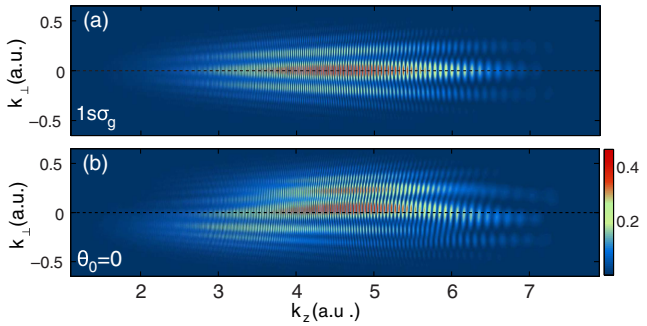

FIG. 1. (a) Photoelectron momentum distribution for tunneling ionization of the ground state ($1s\sigma_g$) H_2^+ by a single-cycle pulse with wavelength of $\lambda = 2000$ nm and intensity of 3.0×10^{14} W/cm^2. (b) Same as (a) but for tunneling ionization of the superposition state of H_2^+ with $\theta_0 = 0$ and $c_2/c_1 = 0.5$.

To reveal the electron dynamics encoded in the holographic fringes, we first wash out the vertical fringes by averaging the PEMDs over k_z with a window function [26]. Cuts of the averaged PEMD from Fig. 1(b) taken at $k_z = 4$ and 6 a.u. as functions of $k_\perp$ are shown in Figs. 2(a) and 2(b), respectively. Results of the $1s\sigma_g$ state are also presented for comparison. For $1s\sigma_g$ state, the positions of the minima and maxima of the modulations are symmetric about $k_\perp = 0$, while for the superposition state a clear shift is visible. For example, for the cut at $k_z = 4$ a.u., the minima at $k_\perp < 0$ side shift toward smaller $|k_\perp|$ and those at $k_\perp > 0$ side shift toward larger $|k_\perp|$. The shift is reversed for the cut at $k_z = 6.0$ a.u., shown in Fig. 2(b).

The holographic fringes are determined by the phase difference between the direct and the rescattering electrons. In the adiabatic theory [24,37], this phase difference is written as [26]

$$\Delta\varphi(k_\perp) = \frac{1}{2}k_\perp^2(t_{r0} - t_{i0}) + \alpha + [\phi_s(0; t_{i0}) - \phi_s(k_\perp; t_{i0})]. \quad (1)$$

Here, t_{i0} and t_{r0} are the ionization and rescattering times, respectively. The three terms on the right-hand side have transparent physical meanings. The first term $\frac{1}{2}k_\perp^2(t_{r0} - t_{i0})$ corresponds to the phase difference between the direct and rescattering electrons accumulated during their propagation in the laser field. This term has been revealed by the strong-field approximation and the semiclassical model [20,38,39]. The

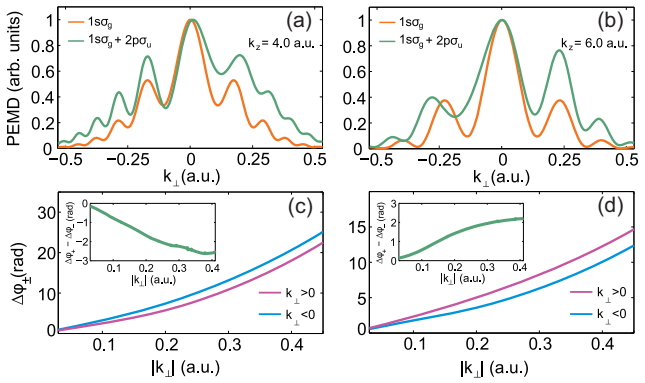

FIG. 2. Cuts of averaged PEMDs for the ground state (orange curve) and the superposition state with initial relative phase $\theta_0 = 0$ (green curve) at (a) $k_z = 4.0$ and (b) $k_z = 6.0$ a.u. (c) The phase difference $\Delta\varphi_{+,-}$ for $k_\perp > 0$ (purple curve) and $k_\perp < 0$ (blue curve) extracted from the cuts (green curve) in (a). The inset presents the quantity $\Delta\varphi_+ - \Delta\varphi_-$ as a function of $|k_\perp|$. (d) Same as (c) but for the PEMD in (b).

second term α is the phase of the scattering amplitude [24]. The third term relates to the phase of the transverse momentum distribution amplitude of tunneling ionization

$$\phi_s(k_\perp; t_{i0}) = \arg[c_1 A_1(k_\perp; t_{i0}) + c_2 A_2(k_\perp; t_{i0}) e^{-i\theta(t_{i0})}], \tag{2}$$

where $A_{1,2}$ represent the transverse momentum distribution amplitudes of $1s\sigma_g$ and $2p\sigma_u$ states [40], respectively. $\theta(t_{i0})$ denotes the time-dependent relative phase between the $1s\sigma_g$ and $2p\sigma_u$ states. Note that for the stationary state that is symmetric ($1s\sigma_g$) or antisymmetric ($2p\sigma_u$) with respect to the laser polarization axis, $\phi_s(0; t_{i0}) - \phi_s(k_\perp; t_{i0}) = 0$ and thus it disappears in Eq. (1). For the nonstationary superposition state, $\phi_s(0; t_{i0}) - \phi_s(k_\perp; t_{i0})$ is a nontrivial phase. It carries the electronic dynamic information of the nonstationary superposition state through the argument $\theta(t_{i0})$.

To retrieve the electronic dynamics from the hologram, we extract the phase differences $\Delta\varphi_\pm$ from the PEMDs [26], as shown in Figs. 2(c) and 2(d). Here, $\Delta\varphi_\pm$ denote $\Delta\varphi(k_\perp)$ for $k_\perp > 0$ and $k_\perp < 0$, respectively. Because of the symmetry of our system, the first and second terms in Eq. (1) for $k_\perp > 0$ and $k_\perp < 0$ are exactly equal, and thus these terms can be eliminated safely by performing a subtracting procedure $\Delta\varphi_+ - \Delta\varphi_- = \phi_s(-|k_\perp|) - \phi_s(|k_\perp|)$. With this procedure, the phase of the transverse momentum distribution amplitude could be retrieved without the knowledge of the laser parameters and the phase of the scattering amplitude α. The obtained quantity $\Delta\varphi_+ - \Delta\varphi_-$ for $k_z = 4.0$ a.u. and $k_z = 6.0$ a.u. are displayed in the insets of Figs. 2(c) and 2(d), respectively. It decreases with $|k_\perp|$ for $k_z = 4.0$ a.u. and increases for $k_z = 6.0$ a.u.. This k_z-dependence behavior indicates that the electronic dynamics of nonstationary superposition state is indeed encoded in and can be extracted from the photoelectron hologram. With the extracted quantity $\phi_s(-|k_\perp|) - \phi_s(+|k_\perp|)$, the two free parameters c_2/c_1 and $\theta(t_{i0})$ are retrieved based on Eq. (2) by the nonlinear least-squares fitting. The fitting procedure requires the basis functions $A_1(k_\perp)$ and $A_2(k_\perp)$, which can be accurately calculated [40,41]. The basis functions in our fitting are shown in Fig. 3(a).

The above procedure can be repeated for different k_z. Several example curves for the extracted quantity $\Delta\varphi_+ - \Delta\varphi_-$ together with the fitted ones at different k_z are shown in Fig. 3(b). Mapping the momentum k_z to the ionization time t_{i0} with the relation $k_z = -\int_{t_{i0}}^{\infty} F(t')dt'$, where $F(t')$ is the electric field of the laser pulse, the fitting parameters c_2/c_1 and $\theta(t_{i0})$ as a function of time are obtained. Note that in our calculation the range of momentum k_z corresponds to a time interval of 600 as, which is about the half oscillating period of the field-free superposition state. In order to visualize the electron motion during the whole oscillating period, we also use the PEMD for $\theta_0 = \pi$. The initial phase θ_0 is equivalent to a time delay in the pump-probe experiments. Figure 3(c) shows the retrieved $\theta(t_{i0})$,

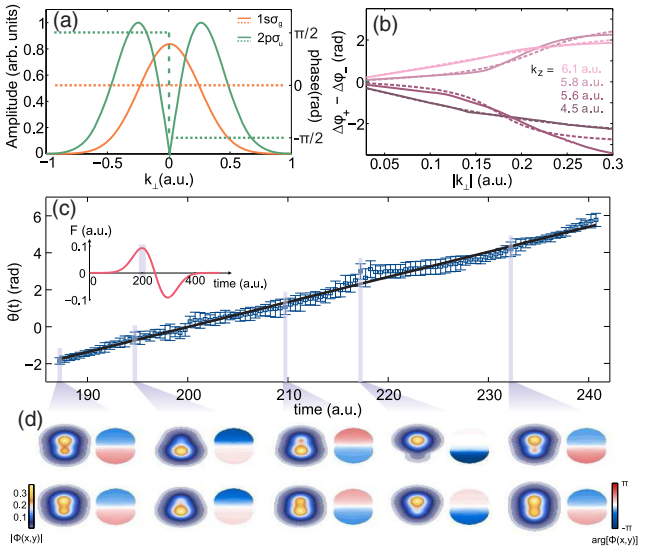

FIG. 3. (a) The transverse momentum distribution amplitude of $1s\sigma_g$ (orange) and $2p\sigma_u$ (green) states of H_2^+, respectively. The magnitudes and phases are represented by solid (left ordinate) and dashed (right ordinate) curves, respectively. (b) The phase difference $\Delta\phi_+ - \Delta\phi_-$ extracted from the PEMD in Fig. 1(b) at four different k_z. Dotted lines are the fitted results using the bases in (a). (c) The retrieved relative phase θ of the superposition state as a function of time (blue squares). The black line is the linear fitting of $\theta(t)$. The inset presents the electric field used in our calculations. The shadowed area indicates the time window where the electron dynamics is retrieved from the PEMDs. The error bars indicate the 95% confidence interval in fitting. (d) The reconstructed modulus (left) and phase (right) of electron wave functions at selected instants marked with solid squares in (c). The lower row of (d) shows the field-free evolution of the superposition state wave function for comparison.

which is a perfect linear function of time with a slope of 0.135 ± 0.002 a.u. This slope is very close to the energy separation of the field-free $1s\sigma_g$ and $2p\sigma_u$ states ($\Delta E = 0.141$ a.u.), meaning that the laser field hardly affects the energy separation of the two states for the perpendicular alignment. This conclusion is the same as other linear molecules reported in previous experiments [13,15]. The retrieved c_2/c_1 is 0.60 ± 0.09, very close to the exact value of 0.5. With these retrieved parameters, the wave functions of the superposition state at sampled times within one oscillating period are reconstructed, as shown in Fig. 3(d). The field-free evolution of the superposition state is also shown for comparison. The reconstructed wave functions, both the modulus and phase, keep in well step with the field-free evolution.

So far, the electron dynamics of the superposition state during the time interval of tunneling ionization has been accurately retrieved with the concept of SFPH. The time resolution of this method is determined by the resolution in the photoelectron momentum k_z. For the current experimental technique, sub-ten attosecond time resolution could be achieved [7].

For more complex molecules, superposition states may involve many electronic states. Usually the wave functions of these involved states are unknown, and even worse it is unclear which states are involved. In this case, the most important dynamics information is the motion of the electron wave packet of this superposition state, i.e., charge migration. Tracing the attosecond charge migration in molecules is one of the most challenging and interesting tasks in attosecond science [42,43]. In the following we will show that SFPH can be used for direct visualization of the attosecond charge migration in molecules without any reconstruction procedure and information about the shape of the involved electronic wave functions, and thus is applicable in complex molecules.

The holographic fringes usually appear at small $k_\perp$. For the state with odd parity, there is a node plane at $k_\perp = 0$ [as shown in Fig. 3(a)], and thus we have $|c_2 A_2(k_\perp)| \ll |c_1 A_1(k_\perp)|$ for $k_\perp \sim 0$. In this case, the phase of the transverse momentum distribution amplitude is written as [26]

$$\phi_s(k_\perp; t_{i0}) \doteq \tan\phi_s(k_\perp; t_{i0}) \doteq \frac{c_2|A_2(k_\perp)|}{c_1|A_1(k_\perp)|}\cos\theta(t_{i0}). \quad (3)$$

In addition, $\{[c_2|A_2(k_\perp)|]/[c_1|A_1(k_\perp)|]\}$ is a nearly linear function of $k_\perp$ for small $|k_\perp|$ (see Fig. S1c in Ref. [26]), and thus $\phi_s(k_\perp; t_{i0}) \doteq \kappa\cos\theta(t_{i0})k_\perp$. This equation suggests that the extracted quantity $\Delta\varphi_+ - \Delta\varphi_-$ should be a nearly linear function of $|k_\perp|$ with a slope of $-2\kappa\cos\theta(t_{i0})$ at small $|k_\perp|$. This is true in Fig. 3(b) for $|k_\perp| < 0.17$ a.u.. To further confirm this point, we perform calculations for a smaller $c_2/c_1 = 0.25$, so that $|c_2 A_2(k_\perp)| \ll |c_1 A_1(k_\perp)|$ is satisfied over a wider range of $|k_\perp|$. The extracted phase difference $\Delta\varphi_+ - \Delta\varphi_-$ is shown in Fig. 4(a). Several cuts from Fig. 4(a) at different k_z are displayed in Fig. 4(b), which indeed are nearly linear functions of $|k_\perp|$. This linear behavior provides a much more intuitive sense on monitoring the attosecond charge migration in molecules. According to the delay theorem of Fourier transformation

$$\mathcal{F}[\psi(y - y_0)] = e^{-iy_0 k_\perp}\mathcal{F}[\psi(y)], \quad (4)$$

a linear phase $-y_0 k_\perp$ in the momentum space corresponds to a shift y_0 of the electron wave packet in coordinates space. Thus, the linear phase in the transverse momentum distribution unambiguously indicates the lateral launch point of the tunneling electron wave packet, i.e., $y_0 = -\kappa\cos\theta(t_{i0})$. This provides a direct observation of the position of the electron wave packet of the superposition state. We perform linear fitting on the phase shown in Fig. 4(a) at each k_z. Figure 4(d) shows the obtained slopes as functions of time. The cosinelike oscillating of the slope reveals the oscillating of position of the valence electron wave packet in the molecule. To check the accuracy of our scheme, we trace field-free time evolution of the electron wave function of the superposition state in Fig. 4(c). The lateral position of maximum density for the electron wave packet at

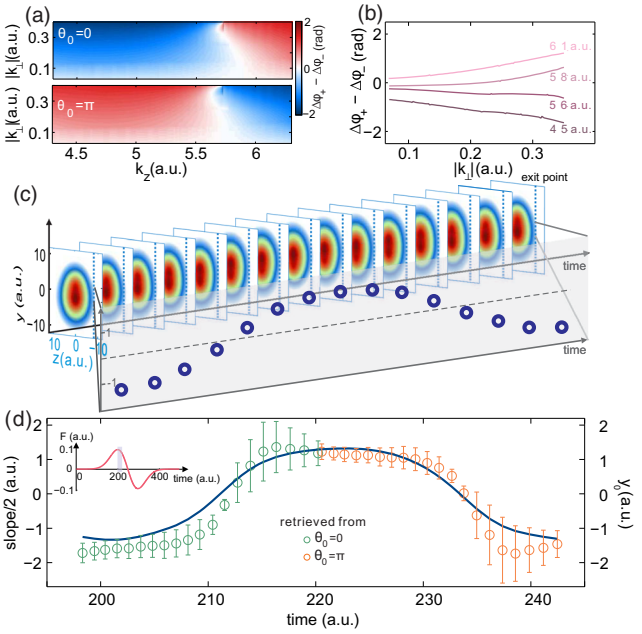

FIG. 4. (a) The phase difference $\Delta\phi_+ - \Delta\phi_-$ extracted from the PEMDs (as presented in the Supplemental Material [26], Fig. S2) for k_z ranging from 4.3 to 6.2 a.u. The upper and lower panels show the results for $\theta_0 = 0$ and π, respectively. Here the superposition state of H_2^+ with populations $c_1 : c_2 = 4 : 1$. (b) Example cuts from the upper panel of (a) for $k_z = 4.5$, 5.6, 5.8, and 6.1 a.u. (c) Back row, electron density distributions in coordinate space as a function of time. The corresponding peak position of electron density distribution at the longitudinal tunneling exit (marked as blue dotted line) is presented as blue cycles in the front row. (d) The position of the oscillating valence electron wave packet retrieved from PEMDs for both $\theta_0 = 0$ (green circles) and π (orange circles). The peak position of electron density distribution at the longitudinal tunneling exit obtained from (c) as a function of time is indicated by the blue solid curve for comparison. The inset presents the electric field used in our calculations. The shadowed area indicates the time window where the electron dynamics is retrieved from the PEMDs. The error bars indicate the 95% confidence interval in fitting.

$z_e = 8.6$ a.u. (around the longitudinal tunneling point [26]) is shown as the solid line in Fig. 4(d). The agreement between the extracted slopes and the positions for the maximum density of the electron wave packet is remarkable. For example, the migration of the electron wave packet from one side of the molecule to the other side during a time interval of 170 as [from 208 a.u. to 215 a.u. in Fig. 4(d)] is tracked with picometer spatial resolution. This establishes an efficient and accurate method to monitor charge migration in molecules with picometer spatial and attosecond temporal resolutions.

Charge migration in molecules is of fundamental importance in biological processes and chemical reactions and has attracted considerable interests during the past years [44–47]. However, direct observation of the attosecond charge migration in real time has not been accessible yet. In

this study, we have illustrated real-time and *in situ* observation of the charge migration with SFPH, where combined picometer spatial and attosecond temporal resolutions are achieved. We mention that with the advanced high-harmonic spectroscopy the attosecond charge migration was reconstructed in a recent experiment [15]. However, in high-harmonic radiation, the tunneling ionization is intrinsically entangled to the continuum electron wave packet propagation and recombination, preventing the direct isolation of the tunneling step, and in the reconstruction procedure the information about the involved states is prerequisite [15]. In this study, we have shown that the transient location of the moving electron wave packet is uniquely mapped to the phase of transverse momentum amplitude in strong-field tunneling ionization. This phase is manifested in the holographic fringes of the PEMD. By extracting this phase from the hologram, the charge migration in molecules is directly visualized without a reconstruction procedure and information of the involved states. Thus, our scheme can be straightforwardly extended to monitor the attosecond charge migration in more complex molecules by directly decoding the phase of the transverse momentum amplitude from the hologram in PEMD. This represents a general and efficient approach for direct observation of the ultrafast electron dynamics in molecules. Furthermore, the hologram also records information of the nuclear dynamics (parametrized by the phase of scattering amplitude α) [24]. Recent experiment has shown the imprint of the coupled electronic and nuclear dynamics in the hologram [19]. Thus our scheme has the potential to probe the coupled nuclear and electronic dynamics in molecules, which will be an exciting prospect.

This work was supported by National Natural Science Foundation of China (Grants No. 11622431, No. 61405064, No. 11722432, No. 61475055, No. 11604108, No. 11234004) and Program for HUST Academic Frontier Youth Team.

*Corresponding author.
zhouymhust@hust.edu.cn
†Corresponding author.
lupeixiang@hust.edu.cn

[1] E. Goulielmakis, Z. Loh, A. Wirth, R. Santra, N. Rohringer, V. S. Yakovlev, S. Zherebtsov, T. Pfeifer, A. M. Azzeer, M. F. Kling, S. R. Leone, and F. Krausz, Real-time observation of valence electron motion, Nature (London) **466**, 739 (2010).

[2] C. Ott, A. Kaldun, L. Argenti, P. Raith, K. Meyer, M. Laux, Y. Zhang, A. Blättermann, S. Hagstotz, T. Ding, R. Heck, J. Madroñero, F. Martín, and T. Pfeifer, Reconstruction and control of a time-dependent two-electron wave packet, Nature (London) **516**, 374 (2014).

[3] M. Schultze, M. Fieß, N. Karpowicz, J. Gagnon, M. Korbman, M. Hofstetter, S. Neppl, A. L. Cavalieri, Y. Komninos, Th. Mercouris, C. A. Nicolaides, R. Pazourek, S. Nagele, J. Feist, J. Burgdörfer, A. M. Azzeer, R. Ernstorfer, R. Kienberger, U. Kleineberg, E. Goulielmakis, F. Krausz, and V. S. Yakovlev, Delay in Photoemission, Science **328**, 1658 (2010).

[4] M. Ossiander, F. Siegrist, V. Shirvanyan, R. Pazourek, A. Sommer, T. Latka, A. Guggenmos, S. Nagele, J. Feist, J. Burgdörfer, R. Kienberger, and M. Schultze, Attosecond correlation dynamics, Nat. Phys. **13**, 280 (2017).

[5] T. Remetter, P. Johnsson, J. Mauritsson, K. Varjú, Y. Ni, F. Lépine, E. Gustafsson, M. Kling, J. Khan, R. López-Martens, K. J. Schafer, M. J. J. Vrakking, and A. L'Huillier, Attosecond electron wave packet interferometry, Nat. Phys. **2**, 323 (2006).

[6] J. Mauritsson *et al.*, Attosecond Electron Spectroscopy Using a Novel Interferometric Pump-Probe Technique, Phys. Rev. Lett. **105**, 053001 (2010).

[7] X. Xie, S. Roither, D. Kartashov, E. Persson, D. G. Arbó, L. Zhang, S. Gräfe, M. S. Schöffler, J. Burgdörfer, Andrius Baltuška, and M. Kitzler, Attosecond Probe of Valence-Electron Wave Packets by Subcycle Sculpted Laser Fields, Phys. Rev. Lett. **108**, 193004 (2012).

[8] V. Gruson, L. Barreau, Á. Jiménez-Galan, F. Risoud, J. Caillat, A. Maquet, B. Carré, F. Lepetit, J.-F. Hergott, T. Ruchon, L. Argenti, R. Taïeb, F. Martín, and P. Salières, Attosecond dynamics through a Fano resonance: Monitoring the birth of a photoelectron, Science **354**, 734 (2016).

[9] H. Niikura, F. Légaré, R. Hasbani, A. Bandrauk, M. Ivanov, D. Villeneuve, and P. Corkum, Sub-laser-cycle electron pulses for probing molecular dynamics, Nature (London) **417**, 917 (2002).

[10] S. Baker, J. Robinson, C. Haworth, H. Teng, R. Smith, C. Chirilă, M. Lein, J. Tisch, and J. Marangos, Probing proton dynamics in molecules on an attosecond time scale, Science **312**, 424 (2006).

[11] W. Li, X. Zhou, R. Lock, S. Patchkovskii, A. Stolow, H. Kapteyn, and M. Murnane, Time-resolved dynamics in N_2O_4 probed using high harmonic generation, Science **322**, 1207 (2008).

[12] P. Lan, M. Ruhmann, L. He, C. Zhai, F. Wang, X. Zhu, Q. Zhang, Y. Zhou, M. Li, M. Lein, and P. Lu, Attosecond Probing of Nuclear Dynamics with Trajectory-Resolved High-Harmonic Spectroscopy, Phys. Rev. Lett. **119**, 033201 (2017).

[13] O. Smirnova, Y. Mairesse, S. Patchkovskii, N. Dudovich, D. Villeneuve, P. Corkum, and M. Ivanov, High harmonic interferometry of multi-electron dynamics in molecules, Nature (London) **460**, 972 (2009).

[14] H. Wörner, J. Bertrand, D. Kartashov, P. Corkum, and D. Villeneuve, Following a chemical reaction using high-harmonic interferometry, Nature (London) **466**, 604 (2010).

[15] P. Kraus, B. Mignolet, D. Baykusheva, A. Rupenyan, L. Horný, E. Penka, G. Grassi, O. Tolstikhin, J. Schneider, F. Jensen, L. Madsen, A. Bandrauk, F. Remacle, and H. Wörner, Measurement and laser control of attosecond charge migration in ionized iodoacetylene, Science **350**, 790 (2015).

[16] C. Blaga, J. Xu, A. DiChiara, E. Sistrunk, K. Zhang, P. Agostini, T. Miller, L. DiMauro, and C. Lin, Imaging ultrafast molecular dynamics with laser-induced electron diffraction, Nature (London) **483**, 194 (2012).

[17] B. Wolter, M. Pullen, A. Le, M. Baudisch, K. Doblhoff-Dier, A. Senftleben, M. Hemmer, C. D. Schröter, J. Ullrich, T. Pfeifer, R. Moshammer, S. Gräfe, O. Vendrell, C. D. Lin, and J. Biegert, Ultrafast electron diffraction imaging of bond breaking in di-ionized acetylene, Science **354**, 308 (2016).

[18] J. Xu, C. I. Blaga, A. D. DiChiara, E. Sistrunk, K. Zhang, Z. Chen, A. T. Le, T. Morishita, C. D. Lin, P. Agostini, and L. F. DiMauro, Laser-Induced Electron Diffraction for Probing Rare Gas Atoms, Phys. Rev. Lett. **109**, 233002 (2012).

[19] S. Walt, N. Ram, M. Atala, N. Shvetsov-Shilovski, A. von Conta, D. Baykusheva, M. Lein, and H. Wörner, Dynamics of valence-shell electrons and nuclei probed by strong-field holography and rescattering, Nat. Commun. **8**, 15651 (2017).

[20] Y. Huismans *et al.*, Time-resolved holography with photoelectrons, Science **331**, 61 (2011).

[21] D. D. Hickstein, P. Ranitovic, S. Witte, X. M. Tong, Y. Huismans, P. Arpin, X. Zhou, K. E. Keister, C. W. Hogle, B. Zhang, C. Ding, P. Johnsson, N. Toshima, M. J. J. Vrakking, M. M. Murnane, and H. C. Kapteyn, Direct Visualization of Laser-Driven Electron Multiple Scattering and Tunneling Distance in Strong-Field Ionization, Phys. Rev. Lett. **109**, 073004 (2012).

[22] M. Meckel, A. Staudte, S. Patchkovskii, D. Villeneuve, P. Corkum, R. Dörner, and M. Spanner, Signatures of the continuum electron phase in molecular strong-field photoelectron holography, Nat. Phys. **10**, 594 (2014).

[23] D. G. Arbó, C. Lemell, S. Nagele, N. Camus, L. Fechner, A. Krupp, T. Pfeifer, S. D. López, R. Moshammer, and J. Burgdörfer, Ionization of argon by two-color laser pulses with coherent phase control, Phys. Rev. A **92**, 023402 (2015).

[24] Y. Zhou, O. I. Tolstikhin, and T. Morishita, Near-Forward Rescattering Photoelectron Holography in Strong-Field Ionization: Extraction of the Phase of the Scattering Amplitude, Phys. Rev. Lett. **116**, 173001 (2016).

[25] M. Haertelt, X. B. Bian, M. Spanner, A. Staudte, and P. B. Corkum, Probing Molecular Dynamics by Laser-Induced Backscattering Holography, Phys. Rev. Lett. **116**, 133001 (2016).

[26] See Supplemental Material at http://link.aps.org/supplemental/10.1103/PhysRevLett.120.133204 for details about the derivation of the formulas, numerical simulation, extraction procedure, and the results for few-cycle pulses, which include Refs. [27–35].

[27] M. Odenweller, N. Takemoto, A. Vredenborg, K. Cole, K. Pahl, J. Titze, L. P. H. Schmidt, T. Jahnke, R. Dörner, and A. Becker, Strong Field Electron Emission from Fixed in Space H_2^+ Ions, Phys. Rev. Lett. **107**, 143004 (2011).

[28] M. Spanner, S. Gräfe, S. Chelkowski, D. Pavičić, M. Meckel, D. Zeidler, A. B. Bardon, B. Ulrich, A. D. Bandrauk, D. M. Villeneuve *et al.*, Coulomb asymmetry and sub-cycle electron dynamics in multiphoton multiple ionization of H_2, J. Phys. B **45**, 194011 (2012).

[29] M. Protopapas, C. H. Keitel, and P. L. Knight, Atomic physics with super-high intensity lasers, Rep. Prog. Phys. **60**, 389 (1997).

[30] M. D. Feit, J. A. Fleck Jr., and A. Steiger, Solution of the Schrödinger equation by a spectral method, J. Comput. Phys. **47**, 412 (1982).

[31] X. M. Tong, K. Hino, and N. Toshima, Phase-dependent atomic ionization in few-cycle intense laser fields, Phys. Rev. A **74**, 031405 (2006).

[32] D. Gabor, A new microscopic principle, Nature (London) **161**, 777 (1948).

[33] D. G. Arbó, E. Persson, and J. Burgdörfer, Time double-slit interferences in strong-field tunneling ionization, Phys. Rev. A **74**, 063407 (2006).

[34] Y. Yin, J. Li, X. Ren, K. Zhao, Y. Wu, E. Cunningham, and Z. Chang, High-efficiency optical parametric chirped-pulse amplifier in BiB_3O_6 for generation of 3 mJ, two-cycle, carrier-envelope-phase-stable pulses at 1.7 μm, Opt. Lett. **41**, 1142 (2016).

[35] S. Teichmann, F. Silva, S. Cousin, M. Hemmer, and J. Biegert, 0.5-keV Soft x-ray attosecond continua, Nat. Commun. **7**, 11493 (2016).

[36] F. Lindner, M. G. Schätzel, H. Walther, A. Baltuška, E. Goulielmakis, F. Krausz, D. B. Milošević, D. Bauer, W. Becker, and G. G. Paulus, Attosecond Double-Slit Experiment, Phys. Rev. Lett. **95**, 040401 (2005).

[37] O. I. Tolstikhin and T. Morishita, Adiabatic theory of ionization by intense laser pulses: Finite-range potentials, Phys. Rev. A **86**, 043417 (2012).

[38] X. B. Bian, Y. Huismans, O. Smirnova, K. J. Yuan, M. J. J. Vrakking, and A. D. Bandrauk, Subcycle interference dynamics of time-resolved photoelectron holography with midinfrared laser pulses, Phys. Rev. A **84**, 043420 (2011).

[39] M. M. Liu, M. Li, C. Wu, Q. Gong, A. Staudte, and Y. Liu, Phase Structure of Strong-Field Tunneling Wave Packets from Molecules, Phys. Rev. Lett. **116**, 163004 (2016).

[40] P. A. Batishchev, O. I. Tolstikhin, and T. Morishita, Atomic Siegert states in an electric field: Transverse momentum distribution of the ionized electrons, Phys. Rev. A **82**, 023416 (2010).

[41] M. Ivanov, M. Spanner, and O. Smirnova, Anatomy of strong field ionization, J. Mod. Opt. **52**, 165 (2005).

[42] F. Calegari, A. Trabattoni, A. Palacios, D. Ayuso, M. Castrovilli, J. Greenwood, P. Decleva, F. Martín, and M. Nisoli, Charge migration induced by attosecond pulses in bio-relevant molecules, J. Phys. B **49**, 142001 (2016).

[43] F. Lépine, M. Ivanov, and M. Vrakking, Attosecond molecular dynamics: fact or fiction, Nat. Photonics **8**, 195 (2014).

[44] F. Remacle and R. D. Levine, An electronic time scale in chemistry, Proc. Natl. Acad. Sci. U.S.A. **103**, 6793 (2006).

[45] A. I. Kuleff, N. V. Kryzhevoi, M. Pernpointner, and L. S. Cederbaum, Core Ionization Initiates Subfemtosecond Charge Migration in the Valence Shell of Molecules, Phys. Rev. Lett. **117**, 093002 (2016).

[46] L. Belshaw, F. Calegari, M. Duffy, A. Trabattoni, L. Poletto, M. Nisoli, and J. Greenwood, Observation of ultrafast charge migration in an amino acid, J. Phys. Chem. Lett. **3**, 3751 (2012).

[47] F. Calegari, D. Ayuso, A. Trabattoni, L. Belshaw, S. De Camillis, S. Anumula, F. Frassetto, L. Poletto, A. Palacios, P. Decleva, J. Greenwood, F. Martín, and M. Nisoli, Ultrafast electron dynamics in phenylalanine initiated by attosecond pulses, Science **346**, 336 (2014).